INORGANIC CHEMISTRY FRONTIERS

RESEARCH ARTICLE

View Article Online
View Journal | View Issue

Cite this: *Inorg. Chem. Front.*, 2025, **12**, 2648

Isovalent cation substitution drives structural transformation and infrared nonlinear optical activity in Eu-based chalcogenides†

Ping Feng,‡[a,b,c,d] Sheng-Hua Zhou,‡[b,c,e] Mao-Yin Ran,[b,c] Bingxuan Li,[b,c] Xin-Tao Wu,[b,c] Hua Lin *[a,b,c,d] and Qi-Long Zhu *[a,b,c,d]

Received 29th December 2024,
Accepted 12th February 2025

DOI: 10.1039/d4qi03346a

rsc.li/frontiers-inorganic

The development of Eu-based chalcogenides with exceptional nonlinear optical (NLO) performance in the infrared (IR) region has garnered increasing attention. However, the design and synthesis of such compounds with non-centrosymmetric (NCS) structures remain a significant challenge. In this study, we report the successful synthesis of a novel quaternary Eu-based chalcogenide, β-EuZnGeS$_4$, achieved through an isovalent cation substitution strategy starting from the ternary parent compound Eu$_2$GeS$_4$. This innovative approach induces a structural transformation from centrosymmetric to non-centrosymmetric, thereby enhancing the NLO properties. β-EuZnGeS$_4$ crystallizes in the orthorhombic *Fdd*2 space group, with a unique two-dimensional $[ZnGeS_4]^{2-}$ layer structure that accommodates Eu^{2+} cations. Notably, β-EuZnGeS$_4$ exhibits a well-balanced set of optical properties, including a remarkable phase-matching second-harmonic generation (SHG) effect, with its maximum SHG value being twice that of AgGaS$_2$ with a 2050 nm laser. Additionally, it exhibits a high laser-induced damage threshold, surpassing AgGaS$_2$ by a factor of 13.1, along with a broad transparency window extending from 0.39 to 23.7 μm. Theoretical calculations further reveal that these outstanding optical properties stem from the synergistic effects of the highly distorted tetrahedral [ZnS$_4$] and [GeS$_4$] motifs within the crystal lattice. This work not only expands the materials database for rare-earth metal chalcogenides but also provides a novel strategy for designing NCS structures with tailored optical properties for a wide range of applications.

Introduction

Nonlinear optical (NLO) materials have garnered unprecedented attention in laser science and technology because of their ability to facilitate frequency conversion in solid-state laser devices.[1] As is widely recognized, an excellent NLO candidate should meet several crucial prerequisites: a sufficient second-harmonic generation (SHG) intensity (d_{eff}), a large energy gap (E_g), a wide optically transparent window, a moderate birefringence (Δn), chemical stability, and availability for obtaining large single crystals.[2] In the infrared (IR) region, numerous vital fields, including optoelectronic instruments, resource exploration, and remote laser communication, have gained widespread attention and interest. Despite the strong d_{eff} exhibited by commercial IR-NLO crystals such as AgGaQ$_2$ (Q = S, Se)[3] and ZnGeP$_2$,[4] which make them suitable for applications in the IR region, they still suffer from limitations in high-power laser systems due to their low laser-induced damage thresholds (LIDT) or detrimental two-photon absorption, primarily attributed to their small E_g. However, integrating these optical performances into a single crystal is extremely challenging because they typically depend on competing structural requirements, such as the trade-off between wide E_g and strong d_{eff}.[5] Therefore, it is of scientific and technological significance to explore new IR-NLO crystals with outstanding comprehensive performance to overcome these challenges.

Rare-earth (RE) element based chalcogenides have garnered significant attention in the IR-NLO field due to their unique f-electron configurations, strong positive charges, and the high coordination numbers of RE cations. These characteristics often result in distinctive NLO responses and exceptional thermal stability, positioning RE-based chalcogenides as a

[a]*College of Chemistry, Fuzhou University, Fuzhou 350002, China*
[b]*Fujian Science & Technology Innovation Laboratory for Optoelectronic Information of China, Fuzhou 350108, China*
[c]*State Key Laboratory of Structural Chemistry, Fujian Institute of Research on the Structure of Matter, Chinese Academy of Sciences, Fuzhou 350002, China. E-mail: linhua@fjirsm.ac.cn, qlzhu@fjirsm.ac.cn*
[d]*Fujian College, University of Chinese Academy of Sciences, Fuzhou 350002, China*
[e]*Resource environment & Clean energy Laboratory, School of Chemistry and Chemical Engineering, Jiangsu University of Technology, Changzhou 213001, China*

†Electronic supplementary information (ESI) available: Additional experimental and theory results, together with additional tables and figures. CCDC 2385100. For ESI and crystallographic data in CIF or other electronic format see DOI: https://doi.org/10.1039/d4qi03346a

‡These authors contributed equally to this work.

promising and active area of research.[6] A number of RE-based chalcogenides with novel non-centrosymmetric (NCS) structures have been discovered, several of which exhibit strong SHG responses, such as $La_2Sr_3Sn_3S_{12}$ (1.4 × $AgGaS_2$@200–250 μm),[7a] La_4InSbS_9 (1.5 × $AgGaS_2$@150–210 μm),[7b] Sm_4GaSbS_9 (3.8 × $AgGaS_2$@46–74 μm),[7c] and $La_6Ga_2GeS_{14}$ (4.8 × $AgGaS_2$@74–106 μm).[7d] While significant progress has been made, challenges remain that hinder the full potential of this material system. These include: (i) optical E_g issues: many of these materials suffer from narrow optical E_g (<2.33 eV), which limits their ability to mitigate harmful two-photon or free-carrier absorption under fundamental 1064 nm laser excitation. (ii) Phase matching challenges: achieving efficient phase matching is difficult due to the small birefringence (Δn), which complicates their use in practical NLO devices. (iii) Synthesis limitations: the difficulty in synthesizing high-quality crystals, particularly those exceeding millimeter-scale dimensions. Therefore, this system still holds significant potential for further development and exploration.

Recently, our research was centered on Eu-based chalcogenides, primarily due to the unique valence state and coordination characteristics of Eu(II) in comparison with other RE(III) elements in IR-NLO materials.[8] Through the facile boron-chalcogen method,[9] we have successfully synthesized a series of promising Eu-based materials. In the course of our ongoing experiments, we obtained a previously reported ternary compound, Eu_2GeS_4.[10] Despite the presence of asymmetric [GeS_4] units within the structure, these units are arranged in an antiparallel configuration, which leads to crystallization in the centrosymmetric (CS) space group. As a result, this compound does not exhibit NLO activity. It is well-established that crystallization in the NCS space group is a prerequisite for a material to become a viable NLO candidate.[11] Among various strategies for obtaining NCS structures, chemical substitution stands out as one of the simplest and most effective approaches, particularly when cation substitution is applied to CS compounds as the parent structure.[12] There are several successful examples of this method: for instance, in the compound CS $Rb_4Hg_2Ge_2S_8$, replacing Rb with Na in a 3 : 1 ratio led to the formation of the NCS $(Na_3Rb)Hg_2Ge_2S_8$.[13] Similarly, by substituting As with Ga in CS $Ba_2AsGaSe_5$, the NCS compound $Ba_2As_2Se_5$ was obtained.[14] Another example includes the substitution of Sb in CS $K_2Sb_4S_7$ with Ag, resulting in the formation of NCS $K_2Ag_3Sb_3S_7$.[15] However, to the best of our knowledge, there have been no reports to date regarding the substitution of RE metals with transition metals to induce a CS-to-NCS structural transformation.

Guided by the considerations mentioned above, a novel quaternary NCS Eu-based chalcogenide, β-$EuZnGeS_4$, was synthesized using an isovalent cation substitution strategy, with the ternary CS compound Eu_2GeS_4 serving as the structural template. As anticipated, β-$EuZnGeS_4$ exhibits a well-balanced set of optical properties, including a significant phase-matching SHG effect (2.0 × $AgGaS_2$@46–74 μm), a high LIDT of 13.1 × $AgGaS_2$, and a broad transparency window ranging from 0.39 to 23.7 μm. These outstanding characteristics position β-$EuZnGeS_4$ as a promising candidate for IR-NLO applications. In this work, we systematically report its synthesis, crystal structure, optical properties, and theoretical calculations.

Results and discussion

Red-brown single crystals of β-$EuZnGeS_4$ were successfully synthesized through a straightforward boron-chalcogen reaction, using a molar ratio of Eu_2O_3 : Zn : Ge : S : B = 1 : 2 :2 : 8 : 2, with a total mass of 500 mg, at a reaction temperature of 1173 K (see the "Experimental section" for detailed synthesis procedures). Elemental distribution maps, obtained *via* scanning electron microscopy (SEM), demonstrate that Eu, Zn, Ge, and S are uniformly distributed throughout the crystal structure (Fig. 1a). Energy-dispersive X-ray (EDX) spectroscopy analysis further confirmed that the elemental composition of the synthesized crystals matches the stoichiometric formula determined from single-crystal X-ray diffraction (XRD) data (Fig. S1†). Powder XRD patterns confirm the high purity of the synthesized β-$EuZnGeS_4$ crystals (Fig. 1b). Thermal stability was assessed using thermogravimetric-differential thermal analysis (TG-DTA), which showed that β-$EuZnGeS_4$ remains thermally stable up to 1073 K, as depicted in Fig. 1c. This indicates the compound's excellent stability at elevated temperatures, further enhancing its suitability for high-performance applications in nonlinear optics and other fields. To investigate their optical properties, UV–vis–NIR diffuse reflectance spectra of β-$EuZnGeS_4$ and Eu_2GeS_4 were recorded and are shown in Fig. 1d and S2.† The diffuse reflectance spectra were converted to absorbance data using the Kubelka–Munk function.[16] The experimental optical E_g for β-$EuZnGeS_4$ and Eu_2GeS_4 were determined to be 2.42 eV and 2.17 eV, respectively, which are in good agreement with their crystal colors. Notably, these values are higher than those reported for most Eu-based IR-NLO materials, such as $EuHgGeSe_4$ (E_g = 1.97 eV),[17] $EuHgGeS_4$ (E_g = 2.04 eV),[18] $EuHgSnS_4$ (E_g = 2.14 eV),[17] and $EuCdGeSe_4$ (E_g = 2.25 eV).[19] Moreover, Fig. S3† displays the variation of E_g as a function of unit cell volume (V $Å^{-3}$) for the phases in the X^{II}–M^{II}–$M^{IV}Q_4$ (X^{II} = Eu, Sr, Ba; M^{II} = Zn, Cd, Hg; M^{IV} = Si, Ge, Sn; Q = S, Se) family with the space group *Fdd*2. When all compounds are considered, the coefficient of determination (R^2) is 0.455. However, excluding the Eu-based materials increases the R^2 to 0.658. Some similar linear relationships are observed in the A-M^{II}_4-M^{III}_5-Q_{12} and A_2-M^{II}-M^{IV}_3-Q_8 systems.[20,21] As shown in the inset map in Fig. 1d, millimeter-sized single crystals of β-$EuZnGeS_4$ were successfully grown, and the crystals exhibit excellent air stability, maintaining their integrity for over 6 months without noticeable degradation (see Fig. S4† for details). Furthermore, β-$EuZnGeS_4$ exhibits a broad optical transparency spanning the range of 0.39 to 23.7 μm (Fig. 1e), making it a promising candidate for a variety of optical applications. Additionally, two distinct absorption peaks are observed in the 16–21 μm range. The energy of the absorptions in this region is too high to correspond to any vibrational or phonon modes of

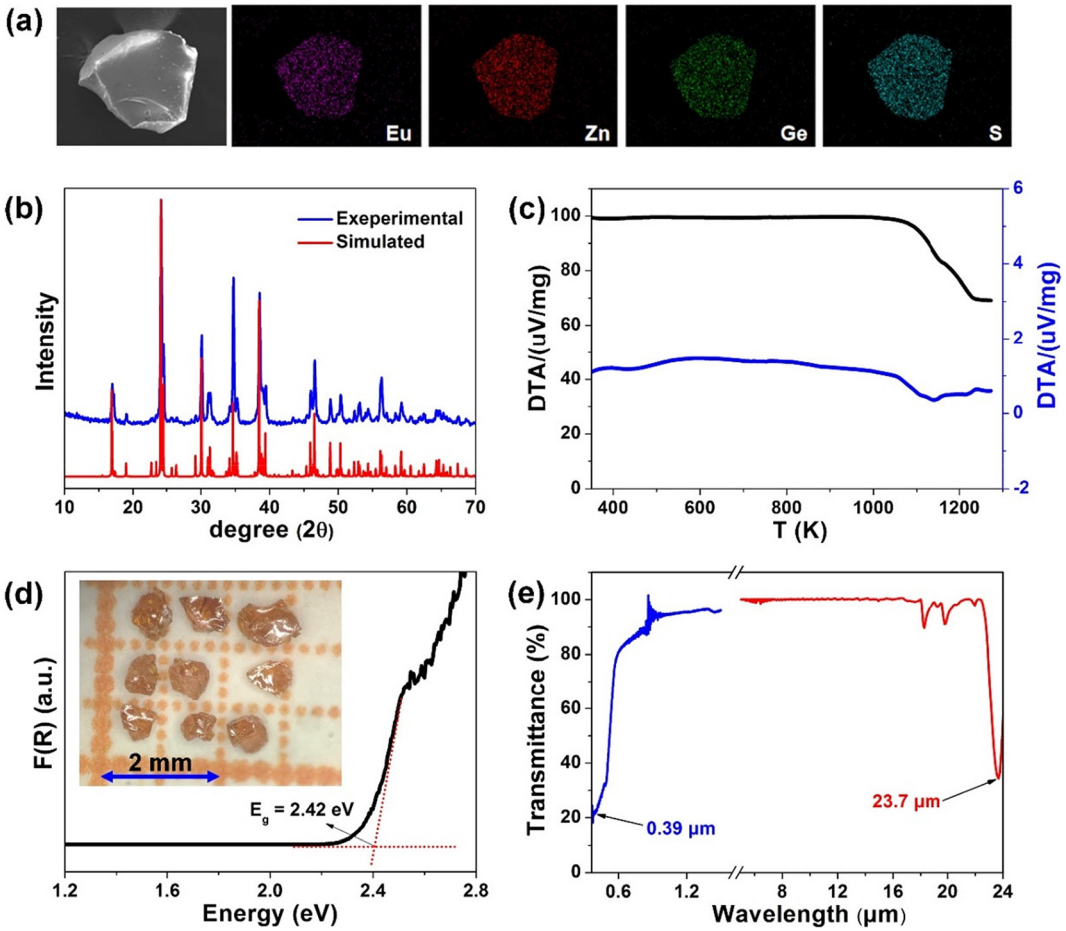

Fig. 1 Experimental characterization results of β-$EuZnGeS_4$: (a) SEM image and corresponding elemental distribution maps; (b) experimental (blue) and simulated (red) powder XRD patterns; (c) TG-DTA test curves; (d) UV–vis–NIR spectrum (inset: photograph of the title crystals); and (e) optical transmittance spectrum.

β-$EuZnGeS_4$. These absorptions may instead be related to the low-frequency phonon modes of the lattice.

The ternary maternal structure of Eu_2GeS_4 belongs to the monoclinic system and contains two unique Eu atoms (Wyckoff site: 2*e*), one unique Ge atom (Wyckoff site: 2*e*), and three unique S atoms (Wyckoff sites: 2*e* and 4*f*) in the asymmetric unit. In this structure, the Ge^{4+} cation occupies the center of its regular tetrahedron, with Ge–S bond lengths ranging from 2.203 to 2.212 Å and ∠S–Ge–S bond angles spanning from 100.55° to 115.63°. When the Eu–S bonds are excluded, the Eu_2GeS_4 structure exhibits a pseudo-zero-dimensional (0D) arrangement, as all the $[GeS_4]$ tetrahedral units are isolated, with counterbalancing Eu^{2+} cations located between them (Fig. 2a). Unfortunately, the $[GeS_4]$ tetrahedra in the structure are arranged centrosymmetrically in a reverse orientation, leading to the cancellation of microscopic second-order polarizability. Consequently, Eu_2GeS_4 does not exhibit NLO activity.

Single-crystal XRD analysis of β-$EuZnGeS_4$ reveals that it crystallizes in the orthorhombic system, specifically within the NCS space group *Fdd*2 (no. 43), with a Pearson symbol of *oF*240 and an idealized Wyckoff sequence of a^2b^{13}. The unit cell parameters are a = 20.6941(8) Å, b = 20.4059(6) Å, and c = 12.2283(4) Å (Table S1†). The asymmetric unit contains three crystallographically independent Eu atoms (occupying Wyckoff sites 8*a* and 16*b*), two independent Zn atoms (Wyckoff site 16*b*), two independent Ge atoms (Wyckoff site 16*b*), and eight independent S atoms (Wyckoff site 16*b*). The atomic parameters and selective bond lengths, summarized in Tables S2 and S3,† reveal bond distances ranging from 2.292 to 2.407 Å for tetrahedral $[ZnS_4]$ units and from 2.194 to 2.234 Å for tetrahedral $[GeS_4]$ units. These values are in good agreement with those reported for similar Zn- and Ge-based chalcogenides.[22] As shown in Fig. 2b, β-$EuZnGeS_4$ is constructed by filling the voids within 2D $[ZnGeS_4]^{2-}$ layers, which extend along the *ab* plane, with charge-balanced Eu^{2+} cations. Fig. 2c illustrates that adjacent $[ZnS_4]$ and $[GeS_4]$ tetrahedra (a total of six) are interconnected through vertex and edge-sharing, forming $[Zn_3Ge_3S_{16}]^{14-}$ 12-membered rings (12-MRs). These 12-MR $[Zn_3Ge_3S_{16}]^{14-}$ rings further link together by corner-sharing to create a 2D $[ZnGeS_4]^{2-}$ layer that extends along the *bc* plane, as highlighted in the red-shaded area in Fig. 2d.

The structural evolution from the ternary CS Eu_2GeS_4 to the quaternary NCS β-$EuZnGeS_4$, achieved through an isovalent

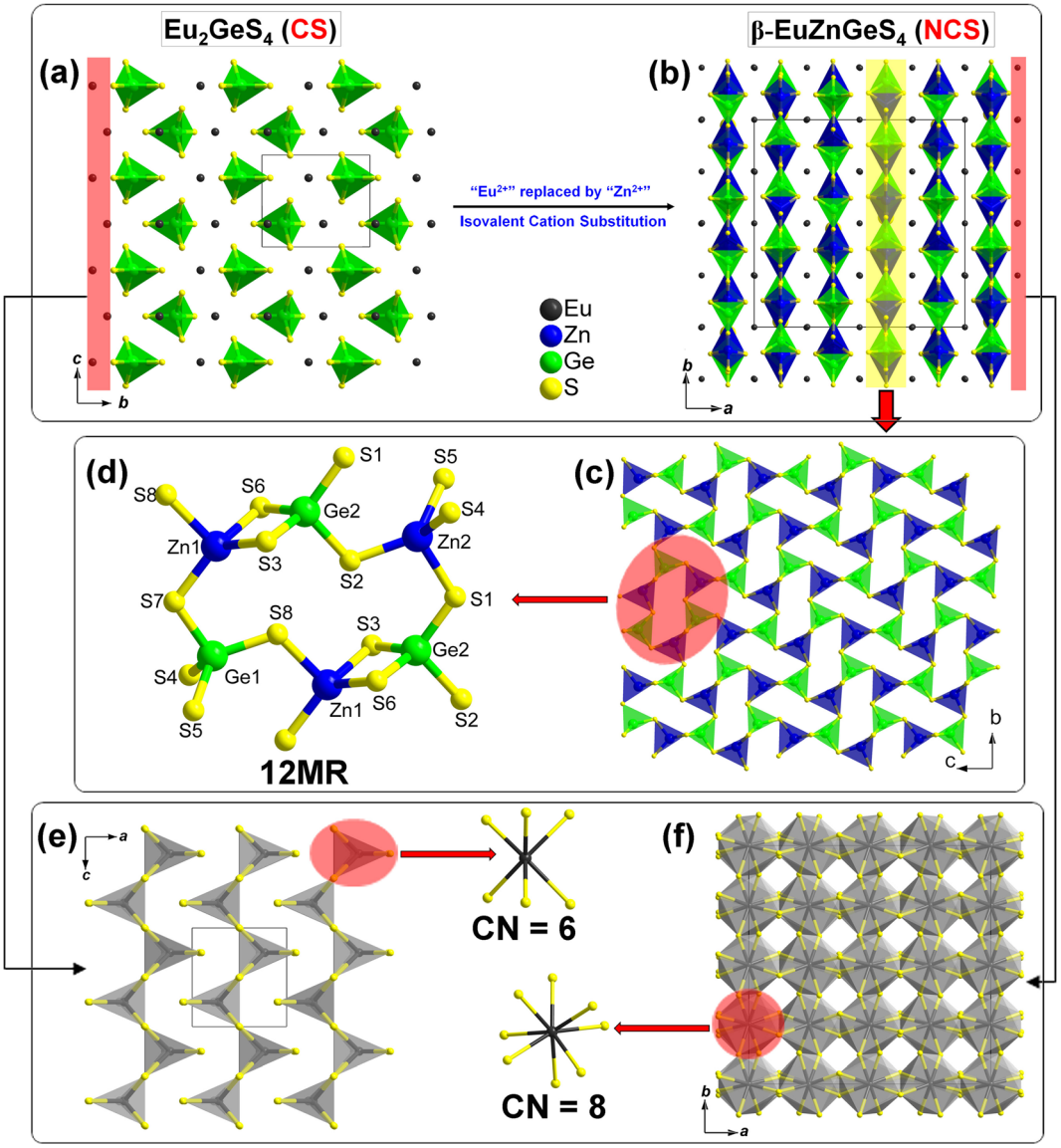

Fig. 2 Structure evolution from ternary CS Eu_2GeS_4 to quaternary NCS β-$EuZnGeS_4$ through an isovalent cation substitution strategy: (a) view of the 0D isolated structure of Eu_2GeS_4 along the *bc* plane (Eu–S bonds are omitted); (b) view of the 2D layered structures of β-$EuZnGeS_4$ along the *ab* plane (Eu–S bonds are omitted); (c) view of the 2D $[ZnGeS_4]^{2-}$ layer of β-$EuZnGeS_4$ along the *bc* plane with the (d) 12-MR rings $[Zn_3Ge_3S_{16}]^{14-}$ marked; (e) a 2D Eu–S layer in the Eu_2GeS_4 composed of polyhedral $[EuS_6]$ motifs; and (f) 3D Eu–S framework in β-$EuZnGeS_4$ composed of polyhedral $[EuS_8]$ motifs.

cation substitution strategy, is depicted in Fig. 2. The choice of substituting Eu^{2+} with Zn^{2+} is driven by two key considerations: first, from a structural perspective, the ionic radii of Eu^{2+} and Zn^{2+} differ significantly, leading to distinct coordination preferences. Eu^{2+}, with its larger ionic radius, tends to form multiple coordination numbers (CNs), while Zn^{2+}, with a smaller ionic radius, favors the formation of 4-coordination structures. This difference in coordination preferences is crucial for disrupting the original CS structure and enabling the formation of an NCS structure. Second, from a functional standpoint, the introduction of Zn^{2+}, a d^{10} cation with a relatively small covalent radius, into the crystal structure has been shown to increase the E_g while maintaining a relatively large SHG effect.[23] This effect has been previously validated in analogous systems, where the incorporation of Zn^{2+} ions enhances the material's NLO properties. These dual structural and functional advantages underscore the rationale for selecting Zn^{2+} as an isovalent substitute for Eu^{2+} in this context. As anticipated, notable structural changes occurred following the substitution: (i) increased distortion of tetrahedra: the degree of distortion in the $[GeS_4]$ tetrahedra increased significantly, from 0.003 in Eu_2GeS_4 to 0.015 in β-$EuZnGeS_4$. Additionally, the distortion in the newly introduced $[ZnS_4]$ tetrahedra was also more pronounced, with a distortion degree of 0.046. This indicates that the substitution of Zn^{2+} for Eu^{2+} introduces greater geometric flexibility, which is reflected in the increased

distortion of the tetrahedral units. (ii) Changes in the Eu–S bonding and coordination: in CS Eu_2GeS_4, Eu and S form a 2D layered structure, while in NCS β-$EuZnGeS_4$, the Eu–S bonding results in a more complex 3D framework structure. This transition is accompanied by a change in the CN of the Eu atoms, from a coordination number of 6 in Eu_2GeS_4 to 8 in β-$EuZnGeS_4$, as illustrated in Fig. 2e, 2f and S5, S6.†

The discovery of β-$EuZnGeS_4$ completes a long-missing piece in the X^{II}–M^{II}–M^{IV}–Q_4 (X^{II} = Eu, Sr, Ba; M^{II} = Zn, Cd, Hg; M^{IV} = Si, Ge, Sn; Q = S, Se) family.[24] Remarkably, this family includes four distinct NCS structural types, all of which crystallize in orthorhombic space groups (*i.e.*, *Fdd*2 (no. 43), *Ama*2 (no. 40), and *Pnn*2 (no. 34)). These structures share similar unit cell parameters that are capable of doubling, and they possess a polar 2-fold screw axis along the *c*-axis. As illustrated in Fig. 3a, the structures of these compounds can be broadly classified into two categories: (1) 2D structures, formed by various methods of linking 12MR $[M^{II}{}_3M^{IV}{}_3Q_{16}]^{14-}$ rings, and (2) 1D chain structures, consisting of dimers $[M^{II}M^{IV}Q_6]$ connected through shared edges. The relationship between the degree of structural distortion, quantified by Δd and $\Delta\theta$, and the space groups is shown in Fig. 3b and further detailed in Table S4.† The analysis reveals several key trends: (i) within the brown region, where $\Delta d < 0.07$ Å and $\Delta\theta < 22°$, the compounds

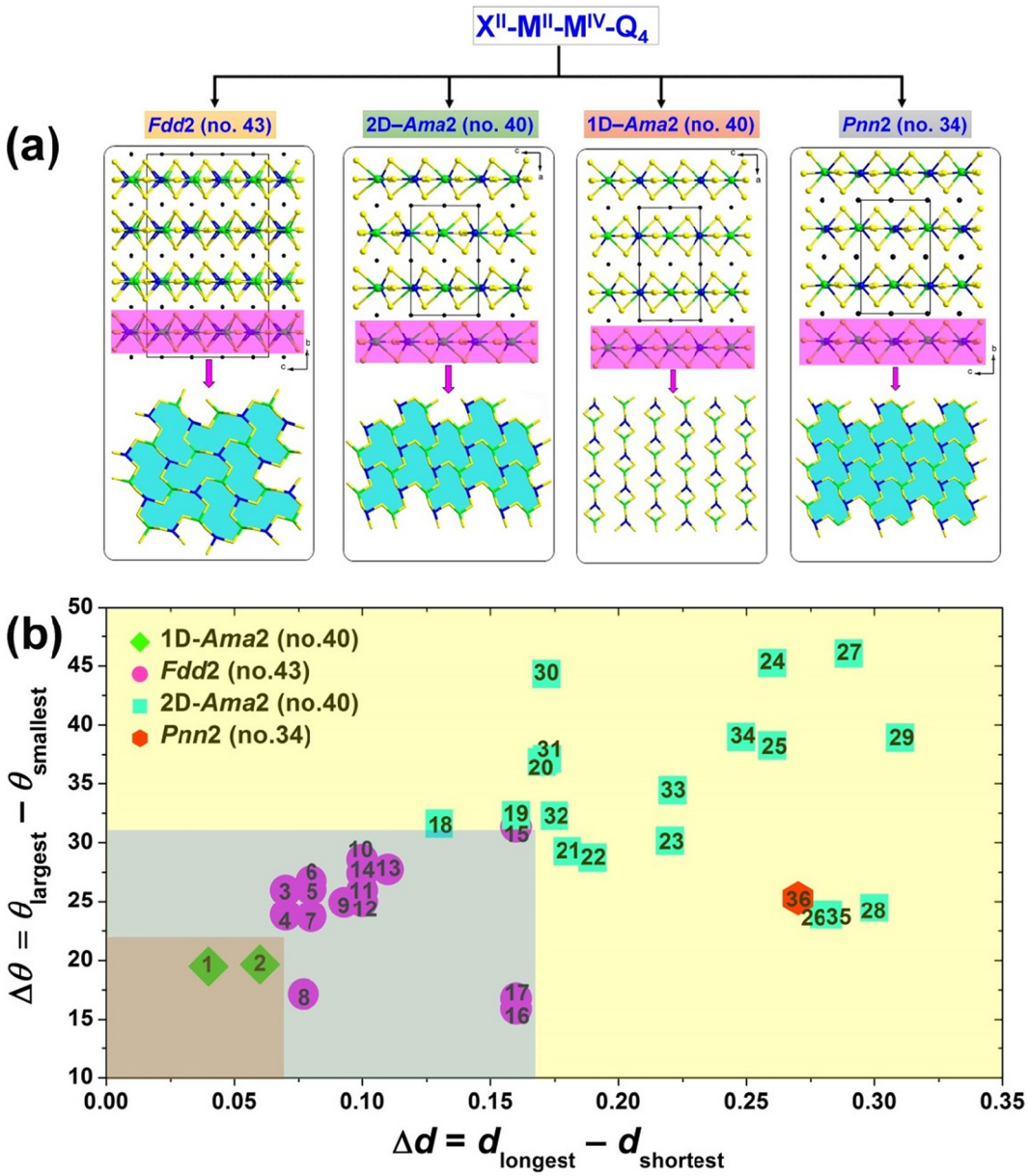

Fig. 3 (a) Comparison of four distinct structural types within the X^{II}–M^{II}–M^{IV}–Q_4 (X^{II} = Eu, Sr and Ba; M^{II} = Zn, Cd, and Hg; M^{IV} = Si, Ge and Sn; Q = S, Se) family; (b) the relationship between the degree of structural distortion, quantified by Δd ($\Delta d = (d_{longest} - d_{shortest})$ and $(\Delta d1 + \Delta d2)/2$), $\Delta\theta$ ($\Delta\theta = (\theta_{largest} - \theta_{smallest})$ and $(\Delta\theta1 + \Delta\theta2)/2$), and the space groups. The compounds corresponding to the numbers in this figure are listed in Table S4.†

crystallize in the *Ama*2 space group, and the anionic groups predominantly form 1D chains; (ii) within the blue region, where $0.07 < \Delta d < 0.17$ Å and $22° < \Delta\theta < 32°$, the compounds adopt the *Fdd*2 space group, with the anionic groups favoring a 2D layered arrangement; and (iii) within the yellow region, where $\Delta d > 0.17$ Å and $\Delta\theta > 32°$, the compounds belong to either the *Ama*2 or *Pnn*2 space group, with anionic groups again forming 2D layers. These findings align with the conclusions drawn by Yu *et al.* in the AE–M^{II}–M^{IV}–Q_4 (AE = alkaline-earth metal) system and underscore the importance of carefully selecting tetrahedral [MQ_4] structural units with varying degrees of distortion. Such an approach enables the design and synthesis of chalcogenides with different space groups within the X^{II}–M^{II}–M^{IV}–Q_4 family. This structural flexibility provides a promising pathway for tailoring optical properties, opening new possibilities for the development of materials with enhanced NLO performance.

Compared to CS α-$EuZnGeS_4$ [space group: *Fddd* (no. 70)], β-$EuZnGeS_4$ crystallizes in the NCS space group *Fdd*2 (no. 43), making it a promising candidate for NLO applications. With the modified Kurtz–Perry method,[25] the SHG intensity of β-$EuZnGeS_4$ was evaluated by irradiating it with a 2050 nm laser, using $AgGaS_2$ as a benchmark. As shown in Fig. 4a, the SHG intensity exhibited a positive correlation with particle size, eventually leveling off, indicating phase-matching behavior. The strongest SHG intensity of β-$EuZnGeS_4$, at a particle size of 46–75 μm, was approximately twice that of $AgGaS_2$, and about 0.8 times that of $AgGaS_2$ at the largest particle size range of 150–210 μm. From these results, the effective SHG coefficient (d_{eff}) was indirectly calculated using the formula: $d_{eff} = d_{eff,R}\,(I^2\omega/I_R{}^2\omega)^{1/2}$, where d_{eff}, $AgGaS_2$ = 13.4 pm V^{-1},[25] yielding a value of 12.1 pm V^{-1} for β-$EuZnGeS_4$. This indicates its strong NLO response and is comparable with those recently reported for RE-based IR-NLO chalcogenides $Nd_3[Ga_3O_3S_3][Ge_2S_7]$ (0.8 × $AgGaS_2$),[26] $LaCaGa_3OS_6$ (0.9 × $AgGaS_2$),[27] $KYGeS_4$ (1.0 × $AgGaS_2$),[28] $K_3HoP_2S_8$ (1.1 × $AgGaS_2$),[29] and $LaCa_2(BS_3)(SiS_4)$ (1.1 × $AgGaS_2$).[30] Another crucial parameter for NLO materials is the LIDT, which is important for high-power laser applications. The powder LIDT was measured by gradually increasing the laser output energy until material damage was observed under an optical microscope.[31] The LIDT of polycrystalline β-$EuZnGeS_4$ was found to be 36.94 MW cm^{-2}, approximately 13.1 times that of commercial $AgGaS_2$ (2.83 MW cm^{-2}) under identical conditions. This LIDT value is competitive with those of other recently reported IR-NLO crystals, such as $[Ba_4(Ba_6S)][(VO_3S)_6]$ (7.65 × $AgGaS_2$),[32] $LiCaPS_4$ (10 × $AgGaS_2$),[33] $LaBS_3$ (14 × $AgGaS_2$),[34] and $Sr_2GeGa_2OS_6$ (12.4 × $AgGaS_2$).[35] Additionally, Fig. 4b compares the comprehensive NLO performance of β-$EuZnGeS_4$ with that of the commercial benchmark $AgGaS_2$. The larger the area of the radar chart, the better the overall optical performance. Notably, β-$EuZnGeS_4$ outperforms $AgGaS_2$ in several key aspects: it demonstrates a favorable phase-matching (PM) feature, a strong SHG response (0.8 × $AgGaS_2$), a giant LIDT (13.1 × $AgGaS_2$), a sufficient bandgap (E_g > 2.33 eV), and an exceptionally broad IR transmission cut-off range (0.39–23.7 μm). These properties make β-$EuZnGeS_4$ a promising material for advanced IR-NLO applications.

To gain a deeper understanding of the relationship between the crystal structure and the properties of β-$EuZnGeS_4$, we performed first-principles density functional theory (DFT) calculations to investigate its microscopic mechanisms, including the E_g, partial density of states (PDOS), frequency-dependent SHG coefficients (d_{ij}), and refractive index dispersion curves, with a focus on the shortest PM cutoff wavelength.[36] The linear optical properties, in terms of the complex dielectric function $\varepsilon(\omega) = \varepsilon_1(\omega) + i\varepsilon_2(\omega)$, were calculated, and optical constants were derived from the imaginary part of the dielectric function $\varepsilon_2(\omega)$ using the Kramers–Kronig transformation (see the "Computational details" for detailed calculation procedures and parameter settings in the ESI† section). As shown in Fig. 5a, the theoretical calculations reveal that the valence band maximum (VBM) and conduction band minimum (CBM) are both located at the same G point, confirming that β-$EuZnGeS_4$ is a direct E_g semiconductor. The theoretical E_g was calculated to be 2.40 eV, which closely matches the experi-

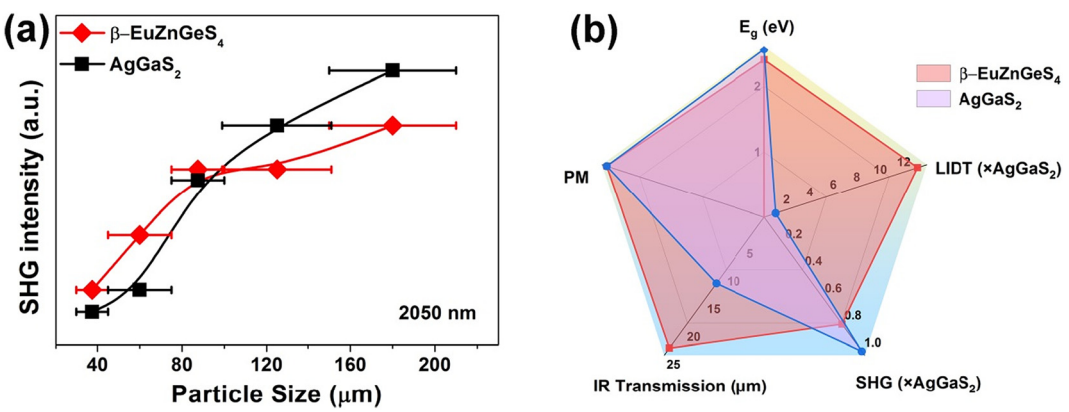

Fig. 4 (a) SHG intensities *vs.* particle size at λ = 2050 nm for β-$EuZnGeS_4$ and $AgGaS_2$; (b) radar chart (five directions representing the PM feature, IR transmission, SHG, LIDT, and E_g, respectively; the colored shadows represent the areas surrounded by these optical parameters of β-$EuZnGeS_4$ and $AgGaS_2$, respectively).

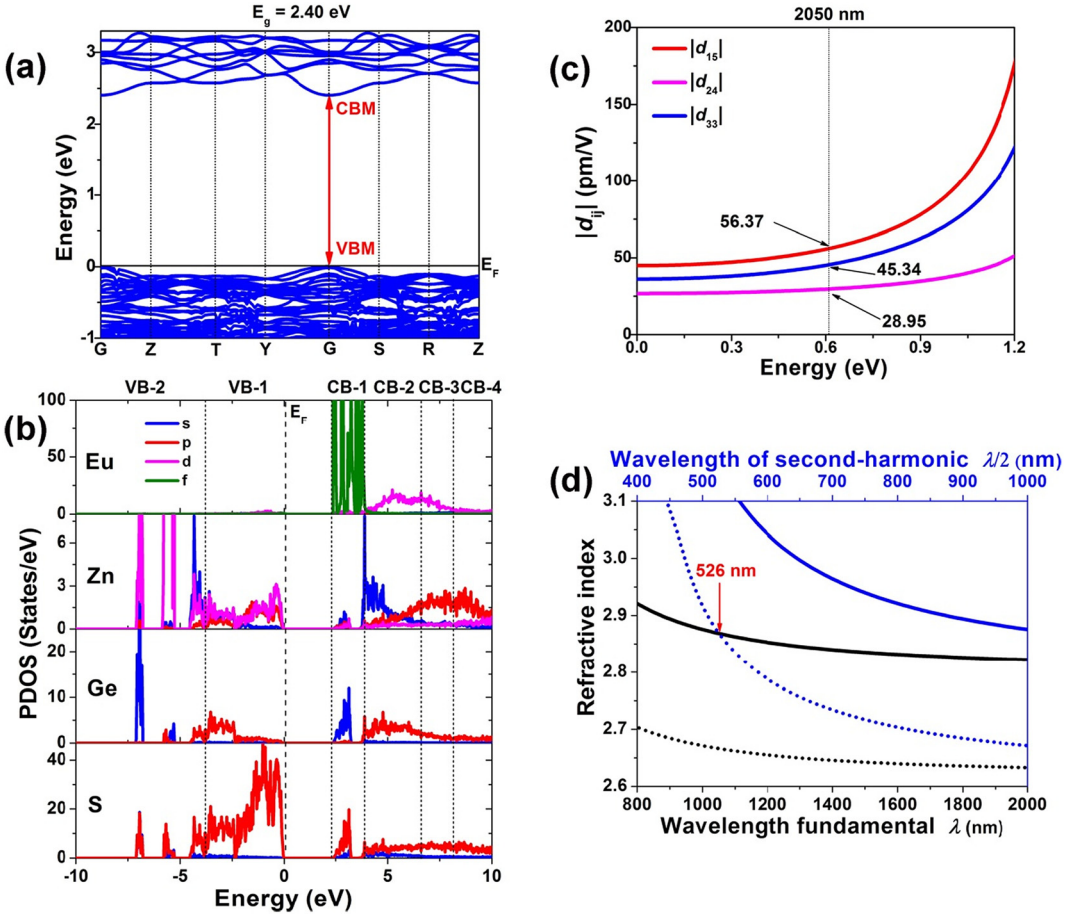

Fig. 5 Theoretical results of electronic structures and optical parameters of β-$EuZnGeS_4$: (a) band structure; (b) partial density of states; (c) calculated nonzero independent SHG coefficient d_{ij} (pm V^{-1}); and (d) calculated refractive index dispersion curves with the shortest type-I PM cut-off wavelength.

mentally measured value of 2.42 eV. The PDOS analysis further elaborates on the energy contributions from various atomic orbitals (Fig. 5b). The valence band (VB-1), near the Fermi level, is primarily composed of Zn-3d, S-3p, and Ge-4p orbitals, while the conduction band (CB-1), also near the Fermi level, is largely influenced by Eu-4f, Zn-4s, Ge-4s, and S-3p orbitals. This analysis highlights the significant role of the $[ZnS_4]$ and $[GeS_4]$ tetrahedral units, particularly the impact of the 2D $[ZnGeS_4]^{2-}$ layers, in determining the electronic structure and, by extension, the optical properties of β-$EuZnGeS_4$.

β-$EuZnGeS_4$ crystallizes in the NCS *Fdd*2 space group and belongs to the *mm*2 point group, which, according to Kleinman's symmetry rule,[37] supports three independent nonzero tensors (d_{15}, d_{24}, and d_{33}) for SHG. As illustrated in Fig. 5c, the theoretical SHG coefficients under a phonon energy of 0.61 eV (corresponding to a 2050 nm wavelength) are d_{15} = 56.37 pm V^{-1}, d_{24} = 45.34 pm V^{-1}, and d_{33} = 28.95 pm V^{-1}. Additionally, the refractive indices along the principal optical axes (n_x, n_y, and n_z) of β-$EuZnGeS_4$ were calculated, revealing significant optical anisotropy, as demonstrated by a Δn value of approximately 0.19 at 2050 nm (Fig. S7†), which is notably larger than that of $AgGaS_2$ (Δn = 0.04 at 2050 nm).[38] This pronounced Δn value suggests that β-$EuZnGeS_4$ can theoretically meet the PM conditions for efficient SHG over a broad wavelength range. The substantial refractive index difference is attributed to the material's unique 2D layered structure, which plays a crucial role in enhancing its optical anisotropy and overall NLO performance. From the PM condition for type-I NLO processes, where $n_e(2\omega) = n_o(\omega)$, the theoretical PM cutoff wavelength for β-$EuZnGeS_4$ was determined to be around 526 nm (Fig. 5d),[39] indicating that this material can efficiently support SHG over a broad spectral range. Together, these insights suggest that β-$EuZnGeS_4$ is a highly promising material for advanced IR-NLO applications, with a strong SHG response, significant optical anisotropy, and favorable PM characteristics.

To investigate the NLO origins of β-$EuZnGeS_4$, we performed detailed calculations on the energy-dependent maximum d_{15} values using the length-gauge formalism,[40] as shown in Fig. 6a. The results reveal that the d_{15} coefficient is primarily governed by electronic transitions involving the VB-1, CB-2, and CB-4 regions. These findings are further supported by PDOS analyses (Fig. 5b) and virtual charge density maps (Fig. 6b), which provide additional insight into the elec-

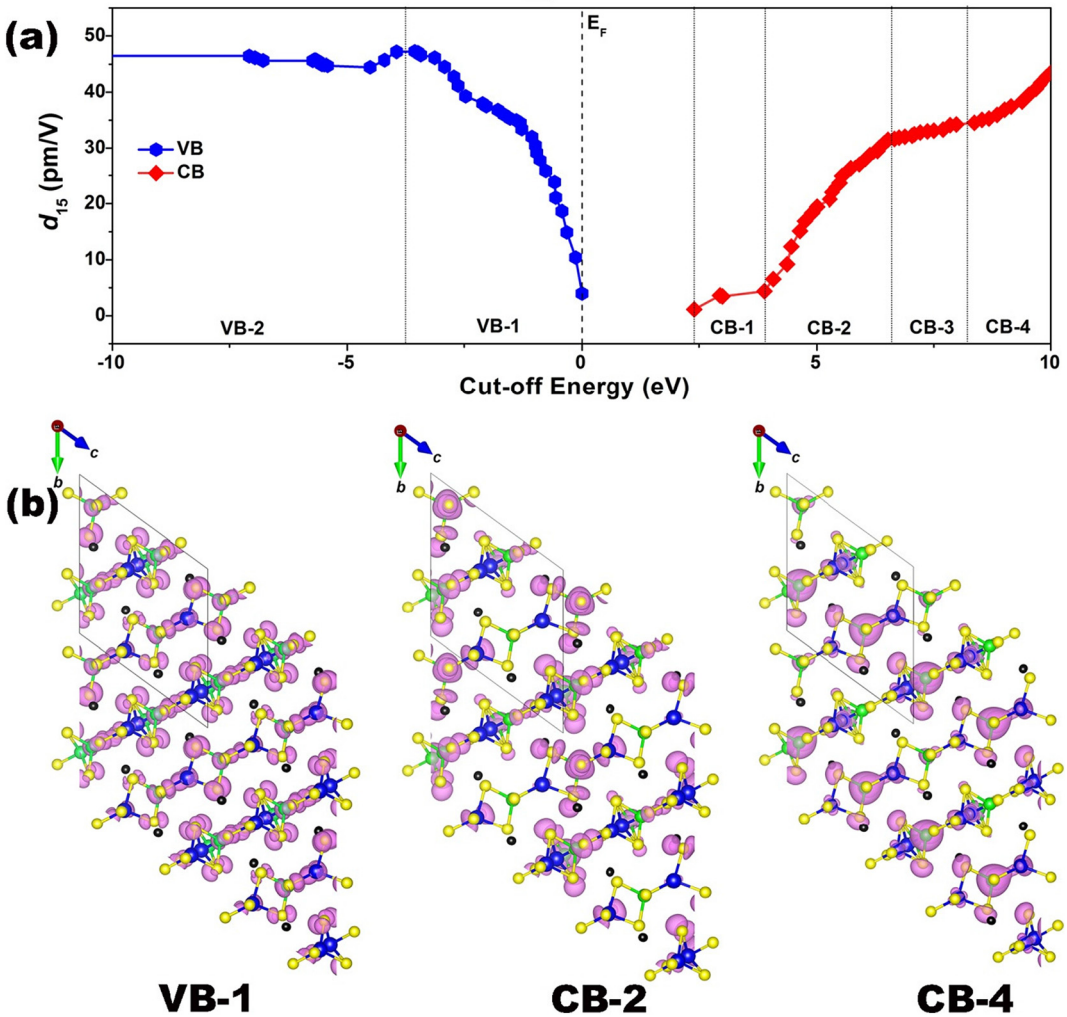

Fig. 6 Theoretical analysis of the intrinsic mechanism of the SHG source for β-$EuZnGeS_4$: (a) cut-off energy (eV) dependence of the static d_{15} (pm V^{-1}) and (b) distribution of the partial charge density maps with major contributions in the VB-1, CB-2 and CB-4 regions. Black atoms: Eu; blue atoms: Zn; green atoms: Ge; and yellow atoms: S.

tronic structure. The PDOS analysis reveals that VB-1 is mainly composed of S-3p and Zn-3d orbitals, while in the conduction bands CB-2 and CB-4 are dominated by Zn-4s, Ge-4p, and S-3p states. Given the distinctive layered structure of the $[ZnGeS_4]^{2-}$ units, the SHG in β-$EuZnGeS_4$ primarily arises from electronic transitions between the fundamental building blocks of the crystal: the $[ZnS_4]$ and $[GeS_4]$ tetrahedral units. The layered arrangement of these building blocks enhances the material's NLO properties by facilitating efficient electronic transitions across different bands, thereby contributing significantly to the observed SHG response.

Conclusions

In summary, we successfully designed a new Eu-based chalcogenide, β-$EuZnGeS_4$, using an isovalent cation substitution strategy and synthesized it *via* the facile boron-chalcogen method. This innovative approach not only facilitates a structural transformation from CS to NCS configurations but also yields impressive NLO properties. Notably, β-$EuZnGeS_4$ exhibits a substantial phase-matching SHG response 0.8 times that of $AgGaS_2$ at 2050 nm, an enhanced LIDT 13.1 times that of $AgGaS_2$ at 1064 nm, and a wide transparency range spanning from 0.39 to 23.7 μm. Additionally, the material demonstrates a significant birefringence of 0.19 at 2050 nm and remarkable thermal stability, withstanding temperatures up to approximately 1073 K. This work highlights β-$EuZnGeS_4$ as a promising candidate for IR-NLO applications within the rarely explored Eu-based chalcogenide system. Furthermore, it is poised to stimulate further research into potential rare-earth metal NLO materials.

Author contributions

Ping Feng: investigation, formal analysis, and writing – original draft. Sheng-Hua Zhou: investigation, methodology, and

validation. Mao-Yin Ran: investigation, formal analysis, and validation. Bingxuan Li: formal analysis and validation. Xin-Tao Wu: conceptualization and writing – review & editing. Hua Lin: supervision, conceptualization, and writing – review & editing. Qi-Long Zhu: supervision and writing – review & editing.

Data availability

The data supporting this article have been included as part of the ESI.†

Crystallographic data for β-$EuZnGeS_4$ have been deposited at the CCDC [2385100]† and can be obtained from **https://www.ccdc.cam.ac.uk/**.

Conflicts of interest

There are no conflicts to declare.

Acknowledgements

This work was supported by the National Natural Science Foundation of China (22175175), Natural Science Foundation of Fujian Province (2022L3092 and 2023H0041), Fujian Science & Technology Innovation Laboratory for Optoelectronic Information of China (2021ZR118), and the Youth Innovation Promotion Association CAS (2022303). The authors thank Professor Yong-Fan Zhang at Fuzhou University for helping with the DFT calculations.

References

1 (*a*) X.-T. Wu and L. Chen, Structure–Property Relationships in Nonlinear Optical Crystals II The IR Region, in *Structure and Bonding*, ed. D. M. Mingos, Springer, New York, 2012, vol. 145, pp. 1–42; (*b*) N. L. B. Sayson, T. Bi, V. Ng, H. Pham, L. S. Trainor, H. G. L. Schwefel, S. Coen, M. Erkintalo and S. G. Murdoch, Octave-spanning tunable parametric oscillation in crystalline Kerr microresonators, *Nat. Photonics*, 2019, **13**, 701–706; (*c*) D. Smirnova and A. B. Khanikaev, Twisted topological light illuminates molecular chirality, *Nat. Photonics*, 2024, **18**, 1133–1134; (*d*) L. Du, Z. Huang, J. Zhang, F. Ye, Q. Dai, H. Deng, G.u. Zhang and Z. Sun, Nonlinear physics of moiré superlattices, *Nat. Mater.*, 2024, **23**, 1179–1192; (*e*) J.-X. Zhang, P. Feng, M.-Y. Ran, X.-T. Wu, H. Lin and Q.-L. Zhu, Ga-based IR nonlinear optical materials: Synthesis, structures, and properties, *Coord. Chem. Rev.*, 2024, **502**, 215617; (*f*) A. Dutt, A. Mohanty, A. L. Gaeta and M. Lipson, Nonlinear and quantum photonics using integrated optical materials, *Nat. Rev. Mater.*, 2024, **9**, 321–346.

2 (*a*) L. Kang, M. Zhou, J. Yao, Z. Lin, Y. Wu and C. Chen, Metal Thiophosphates with Good Mid-infrared Nonlinear Optical Performances: A First-Principles Prediction and Analysis, *J. Am. Chem. Soc.*, 2015, **137**, 13049–13059; (*b*) Y. Pan, S.-P. Guo, B.-W. Liu, H.-G. Xue and G.-C. Guo, Second-order nonlinear optical crystals with mixed anions, *Coord. Chem. Rev.*, 2018, **374**, 464–496; (*c*) M. Mutailipu, K. R. Poeppelmeier and S. Pan, Borates: A Rich Source for Optical Materials, *Chem. Rev.*, 2021, **121**, 1130–1202; (*d*) H. Chen, M.-Y. Ran, W.-B. Wei, X.-T. Wu, H. Lin and Q.-L. Zhu, A comprehensive review on metal chalcogenides with three-dimensional frameworks for infrared nonlinear optical applications, *Coord. Chem. Rev.*, 2022, **470**, 214706.

3 (*a*) A. Harasaki and K. J. Kato, New Data on the Nonlinear Optical Constant, Phase–Matching, and Optical Damage of $AgGaS_2$, *Appl. Phys.*, 1997, **36**, 700–703; (*b*) G. C. Catella, L. R. Shiozawa, J. R. Hietanen, R. C. Eckardt, R. K. Route, R. S. Feigelson, D. G. Cooper and C. L. Marquardt, Mid–IR absorption in $AgGaSe_2$ optical parametric oscillator crystals, *Appl. Opt.*, 1993, **32**, 3948–3951.

4 G. D. Boyd, E. Buehler and F. G. Storz, Linear and nonlinear optical properties of $ZnGeP_2$ and CdSe, *Appl. Phys. Lett.*, 1971, **18**, 301–304.

5 (*a*) K. Wu and S. Pan, A review on structure-performance relationship toward the optimal design of infrared nonlinear optical materials with balanced performances, *Coord. Chem. Rev.*, 2018, **377**, 191–208; (*b*) L. Kang, F. Liang, X. Jiang, Z. Lin and C. Chen, First-Principles Design and Simulations Promote the Development of Nonlinear Optical Crystals, *Acc. Chem. Res.*, 2020, **53**, 209–217; (*c*) W. Wang, D. Mei, F. Liang, J. Zhao, Y. Wu and Z. Lin, Inherent laws between tetrahedral arrangement pattern and optical performance in tetrahedron-based mid-infrared nonlinear optical materials, *Coord. Chem. Rev.*, 2020, **421**, 213444; (*d*) H.-D. Yang, M.-Y. Ran, W.-B. Wei, X.-T. Wu, H. Lin and Q.-L. Zhu, Recent advances in IR nonlinear optical chalcogenides with well-balanced comprehensive performance, *Mater. Today Phys.*, 2023, **35**, 101127; (*e*) W. Zhou and S.-P. Guo, Rational Design of Novel Promising Infrared Nonlinear Optical Materials: Structural Chemistry and Balanced Performances, *Acc. Chem. Res.*, 2024, **57**, 648–660; (*f*) M.-Y. Ran, S.-H. Zhou, W.-B. Wei, B.-X. Li, X.-T. Wu, H. Lin and Q.-L. Zhu, Breaking through the Trade-Off between Wide Band Gap and Large SHG Coefficient in Mercury-based Chalcogenides for IR Nonlinear Optical Application, *Small*, 2024, **20**, 2304563.

6 (*a*) J. Zhao, D. J. Mei, W. K. Wang, Y. D. Wu and D. F. Xue, Recent advances in nonlinear optical rare earth structures, *J. Rare Earths*, 2021, **39**, 1455; (*b*) Z. X. Chen, W. L. Liu and S. P. Guo, A review of structures and physical properties of rare earth chalcophosphates, *Coord. Chem. Rev.*, 2023, **474**, 214870; (*c*) P. Feng, J.-X. Zhang, M.-Y. Ran, X.-T. Wu, H. Lin and Q.-L. Zhu, Rare-earth-based chalcogenides and their derivatives: an encouraging IR nonlinear optical material candidate, *Chem. Sci.*, 2024, **15**, 5869; (*d*) B. Zhang, M.-Y. Ran, X.-T. Wu, H. Lin and Q.-L. Zhu, Recent advances and future perspectives on rare-earth-based nonlinear optical materials with π-conjugated $[XO_3]$ (X = B, C, N) units, *Coord. Chem. Rev.*, 2024, **517**, 216053.

7 (*a*) J. Xu, Y. Xiao, K. Wu, B. Zhang, D. Lu, H. Yu and H. Zhang, Flexible Anionic Groups-Activated Structure Dissymmetry for Strong Nonlinearity in $Ln_2Ae_3MIV_3S_{12}$ Family, *Small*, 2024, **20**, 2306577; (*b*) H. J. Zhao, Y. F. Zhang and L. Chen, Strong Kleinman-Forbidden Second Harmonic Generation in Chiral Sulfide: La_4InSbS_9, *J. Am. Chem. Soc.*, 2012, **134**, 1993; (*c*) M. C. Chen, L. H. Li, Y. B. Chen and L. Chen, In-Phase Alignments of Asymmetric Building Units in Ln_4GaSbS_9 (Ln = Pr, Nd, Sm, Gd–Ho) and Their Strong Nonlinear Optical Responses in Middle IR, *J. Am. Chem. Soc.*, 2011, **133**, 4617; (*d*) Y. F. Shi, Y. K. Chen, M. C. Chen, L. M. Wu, H. Lin, L. J. Zhou and L. Chen, Strongest Second Harmonic Generation in the Polar R_3MTQ_7 Family: Atomic Distribution Induced Nonlinear Optical Cooperation, *Chem. Mater.*, 2015, **27**, 1876.

8 (*a*) X. Huang, S. H. Yang, X. H. Li, W. Liu and S. P. Guo, $Eu_2P_2S_6$: The First Rare–Earth Chalcogenophosphate Exhibiting Large Second–Harmonic Generation Response and High Laser–Induced Damage Threshold, *Angew. Chem., Int. Ed.*, 2022, **61**, e202206791; (*b*) M. Yang, W.-D. Yao, W. Liu and S.-P. Guo, The first quaternary rare-earth oxythiogermanate with second-harmonic generation and ferromagnetic behavior, *Chem. Commun.*, 2023, **59**, 3894; (*c*) P. Feng, S.-H. Zhou, B.-X. Li, J.-X. Zhang, M.-Y. Ran, X.-T. Wu, H. Lin and Q.-L. Zhu, Realizing Excellent Infrared Nonlinear Optical Performance in Eu-Based Chalcogenides via Rational Cross Substitution Strategy, *ACS Appl. Mater. Interfaces*, 2024, **16**, 52682; (*d*) S. Jana, E. A. Gabilondo, M. Mongkhonratanachai, Y. Zhang, P. S. Halasyamani and P. A. Maggard, Large Mid-Infrared Second-Harmonic Generation in Eu(II)-Based Quaternary Chalcogenides, *Chem. Mater.*, 2024, **36**, 9750.

9 (*a*) L. S. Breton, V. V. Klepov and H.-C. zur Loye, Facile Oxide to Chalcogenide Conversion for Actinides using the Boron-Chalcogen Mixture Method, *J. Am. Chem. Soc.*, 2020, **142**, 14365–14373; (*b*) N. Ma, Y.-Y. Li, L. Chen and L.-M. Wu, α-$CsCu_5Se_3$: Discovery of A Low-cost Bulk Selenide with High Thermoelectric Performance, *J. Am. Chem. Soc.*, 2020, **142**, 5293–5303; (*c*) M. M. Chen, S. H. Zhou, W. B. Wei, X. T. Wu, H. Lin and Q. L. Zhu, Phase Matchability Transformation in the Infrared Nonlinear Optical Materials with Diamond-Like Frameworks, *Adv. Opt. Mater.*, 2022, **10**, 2102123; (*d*) M. M. Chen, S. H. Zhou, W. B. Wei, B. X. Li, M. Y. Ran, X. T. Wu, H. Lin and Q. L. Zhu, $RbBiP_2S_6$: A Promising IR Nonlinear Optical Material with a Giant Second-Harmonic Generation Response Designed by Aliovalent Substitution, *ACS Mater. Lett.*, 2022, **4**, 1264–1269; (*e*) H. Chen, M.-Y. Ran, S.-H. Zhou, X.-T. Wu and H. Lin, Ag_2GeS_3: A Diamond-Like Chalcogenide as an IR Nonlinear Optical Material with Outstanding Second-Harmonic Generation Response, *Adv. Opt. Mater.*, 2024, **12**, 2401100; (*f*) A.-Y. Wang, S. H. Zhou, M. Y. Ran, B.-X. Li, X. T. Wu, H. Lin and Q. L. Zhu, $RbPbPS_4$: a promising IR nonlinear optical material achieved by lone-pair-cation-substitution-induced structure transformation, *Inorg. Chem. Front.*, 2024, **11**, 3744–3754.

10 M. Tampier and D. Johrendt, Structural Evidence for Ferroelectricity in Eu_2GeS_4, *J. Solid State Chem.*, 2001, **158**, 343.

11 (*a*) P. S. Halasyamani and K. R. Poeppelmeier, Noncentrosymmetric Oxides, *Chem. Mater.*, 1998, **10**, 2753–2769; (*b*) K. M. Ok, Toward the Rational Design of Novel Noncentrosymmetric Materials: Factors Influencing the Framework Structures, *Acc. Chem. Res.*, 2016, **49**, 2774–2785; (*c*) H. Chen, W.-B. Wei, H. Lin and X.-T. Wu, Transition-metal-based chalcogenides: A rich source of infrared nonlinear optical materials, *Coord. Chem. Rev.*, 2021, **448**, 214154; (*d*) P.-F. Li, J.-G. Mao and F. Kong, A survey of stereoactive oxysalts for linear and nonlinear optical applications, *Mater. Today Phys.*, 2023, **37**, 101197.

12 (*a*) H. Lin, W. B. Wei, H. Chen, X. T. Wu and Q. L. Zhu, Rational design of infrared nonlinear optical chalcogenides by chemical substitution, *Coord. Chem. Rev.*, 2020, **406**, 213150; (*b*) G. Zou and K. M. Ok, Novel ultraviolet (UV) nonlinear optical (NLO) materials discovered by chemical substitution-oriented design, *Chem. Sci.*, 2020, **11**, 5404–5409; (*c*) M.-Y. Ran, A. Y. Wang, W. B. Wei, X.-T. Wu, H. Lin and Q.-L. Zhu, Recent progress in the design of IR nonlinear optical materials by partial chemical substitution: Structural evolution and performance optimization, *Coord. Chem. Rev.*, 2023, **481**, 215059; (*d*) X. Liu, Y.-C. Yang, M.-Y. Li, L. Chen and L.-M. Wu, Anisotropic structure building unit involving diverse chemical bonds: a new opportunity for high-performance second-order NLO materials, *Chem. Soc. Rev.*, 2023, **52**, 8699–8720; (*e*) Z. Yan, J. Fan, S. Pan and M. Zhang, Recent advances in rational structure design for nonlinear optical crystals: leveraging advantageous templates, *Chem. Soc. Rev.*, 2024, **53**, 6568–6599.

13 C. L. Tang, W. H. Xing, F. Liang, M. R. Sun, J. Tang, Z. S. Lin, J. Y. Yao, K. X. Chen, J. Y. Wu, W. L. Yin and B. Kang, Structural modification from centrosymmetric $Rb_4Hg_2Ge_2S_8$ to noncentrosymmetric $(Na_3Rb)Hg_2Ge_2S_8$: mixed alkali metals strategy for infrared nonlinear optical material design, *J. Mater. Chem. C*, 2022, **10**, 3300.

14 M.-M. Chen, Z. Ma, B.-X. Li, W.-B. Wei, X.-T. Wu, H. Lin and Q.-L. Zhu, $M_2As_2Q_5$ (M = Ba, Pb; Q = S, Se): A source of infrared nonlinear optical materials with excellent overall performance activated by multiple discrete arsenate anions, *J. Mater. Chem. C*, 2021, **9**, 1156–1163.

15 C. Liu, S. H. Zhou, Y. Xiao, C. Zhang, H. Lin and Y. Liu, Aliovalent-cation-substitution-induced structure transformation: a new path toward high-performance IR nonlinear optical materials, *J. Mater. Chem. C*, 2021, **9**, 15407–15414.

16 P. Kubelka and F. Munk, Reflection characteristics of paints, *Z. Tech. Phys.*, 1931, **12**, 593–601.

17 W. Xing, C. Tang, N. Wang, C. Li, Z. Li, J. Wu, Z. Lin, J. Yao, W. Yin and B. Kang, $EuHgGeSe_4$ and $EuHgSnS_4$: Two Quaternary Eu-Based Infrared Nonlinear Optical Materials with Strong Second-Harmonic-Generation Responses, *Inorg. Chem.*, 2020, **59**, 18452.

18 M. Yan, Z.-D. Sun, W.-D. Yao, W. Zhou, W. Liu and S.-p. Guo, A highly distorted HgS_4 tetrahedron-induced moderate second-harmonic generation response of $EuHgGeS_4$, *Inorg. Chem. Front.*, 2020, **7**, 2451.

19 W. Xing, N. Wang, Y. Guo, Z. Li, J. Tang, K. Kang, W. Yin, Z. Lin, J. Yao and B. Kang, Two rare-earth-based quaternary chalcogenides $EuCdGeQ_4$ (Q = S, Se) with strong second-harmonic generation, *Dalton Trans.*, 2019, **48**, 17620.

20 (*a*) H. Lin, L. J. Zhou and L. Chen, Sulfides with Strong Nonlinear Optical Activity and Thermochromism: $ACd_4Ga_5S_{12}$ (A = K, Rb, Cs), *Chem. Mater.*, 2012, **24**, 3406–3414; (*b*) H. Lin, L. Chen, L. J. Zhou and L. M. Wu, Functionalization Based on the Substitutional Flexibility: Strong Middle IR Nonlinear Optical Selenides $AX^{II}_4X^{III}_5Se_{12}$, *J. Am. Chem. Soc.*, 2013, **135**, 12914–12921; (*c*) H. Lin, Y. Liu, L. J. Zhou, H. J. Zhao and L. Chen, Strong Infrared NLO Tellurides with Multifunction: $CsXII_4In_5Te_{12}$ (XII = Mn, Zn, Cd), *Inorg. Chem.*, 2016, **55**, 4470–4475; (*d*) H. Lin, H. Chen, Y. J. Zheng, J. S. Yu and L. M. Wu, $AX^{II}_4X^{III}_5Te_{12}$ (A = Rb, Cs; X^{II} = Mn, Zn, Cd; X^{III} = Ga, In): quaternary semiconducting tellurides with very low thermal conductivities, *Dalton Trans.*, 2016, **45**, 17606–17609; (*e*) H. Lin, H. Chen, Y. J. Zheng, J. S. Yu, X. T. Wu and L. M. Wu, Coexistence of Strong Second Harmonic Generation Response and Wide Band Gap in $AZn_4Ga_5S_{12}$ (A = K, Rb, Cs) with 3D Diamond-like Frameworks, *Chem. – Eur. J.*, 2017, **23**, 10407–10412; (*f*) H. Lin, Y. J. Zheng, X. N. Hu, H. Chen, J. S. Yu and L. M. Wu, Non-centrosymmetric Selenides $AZn_4In_5Se_{12}$ (A = Rb, Cs): Synthesis, Characterization and Nonlinear Optical Properties, *Chem. – Asian J.*, 2017, **12**, 453–458; (*g*) M. Zhou, Y. Yang, Y. Guo, Z. Lin, J. Yao, Y. Wu and C. Chen, Hg-Based Infrared Nonlinear Optical Material $KHg_4Ga_5Se_{12}$ Exhibits Good Phase-Matchability and Exceptional Second Harmonic Generation Response, *Chem. Mater.*, 2017, **29**, 7993–8002; (*h*) M. M. Chen, S. H. Zhou, W. B. Wei, X. T. Wu, H. Lin and Q. L. Zhu, $AZn_4Ga_5Se_{12}$ (A = K, Rb, or Cs): Infrared Nonlinear Optical Materials with Simultaneous Large Second Harmonic Generation Responses and High Laser-Induced Damage Thresholds, *Inorg. Chem.*, 2021, **60**, 10038–10046; (*i*) Y. Wang, R. Wang, X. Che, F. Liang, M. Luo, Y. Tang, Y. Cao and F. Huang, Infrared nonlinear optical sulfide $CsCd_4In_5S_{12}$ exhibiting large second harmonic generation response, *J. Mater. Chem. C*, 2022, **10**, 5183–5189; (*j*) M. Sun, W. Xing, S. K. Chen, C. Li, W. Liu, M.-H. Lee and J. Yao, $ACd_4Ga_5Te_{12}$ (A = K, Rb, Cs): Tellurides with a Strong Nonlinear Optical Response and Purple Emission, *Chem. Mater.*, 2023, **35**, 7218–7228; (*k*) X.-Y. Lou, Y. Zhou, W.-F. Chen, X.-M. Jiang, B.-W. Liu and G.-C. Guo, Open honeycomb frameworks of sulphides $AHg_4Ga_5S_{12}$ (A = Rb, Cs) exhibiting infrared nonlinear optical properties, *Dalton Trans.*, 2023, **52**, 4873–4879.

21 (*a*) C. D. Morris, H. Li, H. Jin, C. D. Malliakas, J. A. Peters, P. N. Trikalitis, A. J. Freeman, B. W. Wessels and M. G. Kanatzidis, $Cs_2M^{II}M^{IV}_3Q_8$ (Q = S, Se, Te): An Extensive Family of Layered Semiconductors with Diverse Band Gaps, *Chem. Mater.*, 2013, **25**, 3344–3356; (*b*) X.-N. Hu, L. Xiong and L.-M. Wu, Six New Members of the $A_2M^{II}M^{IV}_3Q_8$ Family and Their Structural Relationship, *Cryst. Growth Des.*, 2018, **18**, 3124–3131; (*c*) L. Gao, Y. Yang, B. Zhang, X. Wu and K. Wu, Triclinic Layered $A_2ZnSi_3S_8$ (A = Rb and Cs) with Large Optical Anisotropy and Systematic Research on the Inherent Structure–Performance Relationship in the $A_2M^{IIB}M^{IV}_3Q_8$ Family, *Inorg. Chem.*, 2021, **60**, 12573–12579; (*d*) A.-Y. Wang, S.-H. Zhou, M.-Y. Ran, X.-T. Wu, H. Lin and Q.-L. Zhu, Regulating the Key Performance Parameters for Hg-based IR NLO Chalcogenides via Bandgap Engineering Strategy, *Chin. Chem. Lett.*, 2024, **35**, 109377.

22 (*a*) H. Chen, Y.-Y. Li, B.-X. Li, P.-F. Liu, H. Lin, Q.-L. Zhu and X.-T. Wu, Salt-Inclusion Chalcogenide $[Ba_4Cl_2][ZnGa_4S_{10}]$: Rational Design of an IR Nonlinear Optical Material with Superior Comprehensive Performance Derived from $AgGaS_2$, *Chem. Mater.*, 2020, **32**, 8012–8019; (*b*) S.-H. Zhou, M.-Y. Ran, W.-B. Wei, A.-Y. Wang, X.-T. Wu, H. Lin and Q.-L. Zhu, Heteroanion-introduction-driven birefringence enhancement in oxychalcogenide $Ba_3M^{II}Ge_3O_2S_8$ (M^{II} = Mn, Cd), *Inorg. Chem. Front.*, 2023, **10**, 5997–6004; (*c*) A.-Y. Wang, S.-H. Zhou, M.-Y. Ran, X.-T. Wu, H. Lin and Q.-L. Zhu, Regulating the Key Performance Parameters for Hg-based IR NLO Chalcogenides via Bandgap Engineering Strategy, *Chin. Chem. Lett.*, 2024, **35**, 109377; (*d*) M.-Y. Ran, S.-H. Zhou, X.-T. Wu, H. Lin and Q.-L. Zhu, The first Hg-based oxychalcogenide $Sr_2HgGe_2OS_6$: achieving balanced IR nonlinear optical properties through synergistic cation and anion substitution, *Mater. Today Phys.*, 2024, **44**, 101442; (*e*) Y.-F. Shi, S.-H. Zhou, Z. Ma, X.-T. Wu, H. Lin and Q.-L. Zhu, From $[Ba_3S][GeS_4]$ to $[Ba_3CO_3][MS_4]$ (M = Ge, Sn): Enhancing optical anisotropy in IR birefringent crystals via functional group implantation, *Chin. J. Struct. Chem.*, 2025, **44**, 100455.

23 (*a*) G. Li, K. Wu, Q. Liu, Z. Yang and S. Pan, $Na_2ZnGe_2S_6$: a new infrared nonlinear optical material with good balance between large second-harmonic generation response and high laser damage threshold, *J. Am. Chem. Soc.*, 2016, **138**, 7422; (*b*) Y.-Y. Li, P.-F. Liu and L.-M. Wu, $Ba_6Zn_7Ga_2S_{16}$: A Wide Band Gap Sulfide with Phase-Matchable Infrared NLO Properties, *Chem. Mater.*, 2017, **29**, 5259; (*c*) H. Lin, H. Chen, Y.-J. Zheng, J.-S. Yu, X.-T. Wu and L.-M. Wu, Coexistence of Strong Second Harmonic Generation Response and Wide Band Gap in $AZn_4Ga_5S_{12}$ (A = K, Rb, Cs) with 3D Diamond-like Frameworks, *Chem. – Eur. J.*, 2017, **23**, 10407–10412; (*d*) G. M. Li, Y. Chu and Z. X. Zhou, From $AgGaS_2$ to Li_2ZnSiS_4: Realizing Impressive High Laser Damage Threshold Together with Large Second-Harmonic Generation Response, *Chem. Mater.*, 2018, **30**, 602; (*e*) H. Lin, B.-X. Li, H. Chen, P.-F. Liu, L. Wu, X.-T. Wu and Q.-L. Zhu, $Sr_5ZnGa_6S_{15}$: a new quaternary non-centrosymmetric semiconductor with a 3D framework structure displaying excellent nonlinear optical performance, *Inorg. Chem. Front.*, 2018, **5**, 1458–1462.

24 (*a*) Q. Q. Liu, X. Liu, L. M. Wu and L. Chen, $SrZnGeS_4$: A Dual-Waveband Nonlinear Optical Material with a Transparency Spanning UV/Vis and Far-IR Spectral Regions, *Angew. Chem., Int. Ed.*, 2022, **61**, e202205587; (*b*) Y. L. Zhang, D. J. Mei, Y. Yang, W. Z. Cao, Y. D. Wu, J. Lu and Z. S. Lin, Rational design of a new chalcogenide with good infrared nonlinear optical performance: $SrZnSnS_4$, *J. Mater. Chem. C*, 2019, **7**, 8556; (*c*) X. Pang, R. Q. Wang, X. L. Che and F. Q. Huang, $SrZnSnSe_4$: Synthesis, crystal structure and nonlinear optical properties, *J. Solid State Chem.*, 2021, **297**, 122092; (*d*) Y. W. Guo, F. Liang, Z. Li, W. H. Xing, Z. S. Lin, J. Y. Yao, A. Mar and Y. C. Wu, $AHgSnQ_4$ (A = Sr, Ba; Q = S, Se): A Series of Hg-Based Infrared Nonlinear-Optical Materials with Strong Second-Harmonic-Generation Response and Good Phase Matchability, *Inorg. Chem.*, 2019, **58**, 10390; (*e*) Y.-J. Lin, B.-W. Liu, R. Ye, X.-M. Jiang, L.-Q. Yang, H.-Y. Zeng and G.-C. Guo, $SrCdSnQ_4$ (Q = S and Se): infrared nonlinear optical chalcogenides with mixed NLO-active and synergetic distorted motifs, *J. Mater. Chem. C*, 2019, **7**, 4459; (*f*) F. Hou, D. Mei, Y. Zhang, F. Liang, J. Wang, J. Lu, Z. Lin and Y. Wu, $SrZnSnSe_4$: A quaternary selenide with large second harmonic generation and birefringence, *J. Alloys Compd.*, 2022, **904**, 163944; (*g*) H.-D. Yang, M.-Y. Ran, S.-H. Zhou, X.-T. Wu, H. Lin and Q.-L. Zhu, Rational designviadual-site aliovalent substitution leads to an outstanding IR nonlinear optical material with well-balanced comprehensive properties, *Chem. Sci.*, 2022, **13**, 10725; (*h*) M. J. Ma, J. H. Dang, Y. D. Wu, X. M. Jiang and D. J. Mei, Optimal Design of Mid-Infrared Nonlinear-Optical Crystals: From $SrZnSnSe_4$ to $SrZnSiSe_4$, *Inorg. Chem.*, 2023, **62**, 6549; (*i*) Y. W. Dou, Y. Chen, Z. Li, A. K. Iyer, B. Kang, W. L. Yin, J. Y. Yao and A. Mar, $SrCdGeS_4$ and $SrCdGeSe_4$: Promising Infrared Nonlinear Optical Materials with Congruent-Melting Behavior, *Cryst. Growth Des.*, 2019, **19**, 1206; (*j*) Y. W. Guo, F. Liang, W. L. Yin, Z. Li, X. Y. Luo, Z. S. Lin, J. Y. Yao, A. Mar and Y. C. Wu, $BaHgGeSe_4$ and $SrHgGeSe_4$: Two New Hg-Based Infrared Nonlinear Optical Materials, *Chem. Mater.*, 2019, **31**, 3034; (*k*) X. Zhang, H. Wu, Z. Hu, J. Wang, Y. Wu and H. Yu, $A^{II}HgM^{IV}S_4$ (A^{II} = Sr, Ba, M^{IV} = Si, Ge): A Series of Materials with Large Second Harmonic Generation Response and Wide Band Gaps, *Adv. Opt. Mater.*, 2023, **12**, 2301735; (*l*) Y. N. Li, Z. X. Chen, W. D. Yao, R. L. Tang and S. P. Guo, Heterovalent cations substitution to design asymmetric chalcogenides with promising nonlinear optical performances, *J. Mater. Chem. C*, 2021, **9**, 8659; (*m*) Y.-J. Lin, R. Ye, L.-Q. Yang, X.-M. Jiang, B.-W. Liu, H.-Y. Zeng and G.-C. Guo, $BaMnSnS_4$ and $BaCdGeS_4$: infrared nonlinear optical sulfides containing highly distorted motifs with centers of moderate electronegativity, *Inorg. Chem. Front.*, 2019, **6**, 2365; (*n*) N. Zhen, K. Wu, Y. Wang, Q. Li, W. H. Gao, D. W. Hou, Z. H. Yang, H. D. Jiang, Y. J. Dong and S. L. Pan, $BaCdSnS_4$ and $Ba_3CdSn_2S_8$: syntheses, structures, and non-linear optical and photoluminescence properties, *Dalton Trans.*, 2016, **45**, 10681; (*o*) K. Wu, X. Su, Z. H. Yang and S. L. Pan, An investigation of new infrared nonlinear optical material: $BaCdSnSe_4$, and three new related centrosymmetric compounds: Ba_2SnSe_4, Mg_2GeSe_4, and $Ba_2Ge_2S_6$, *Dalton Trans.*, 2015, **44**, 19856; (*p*) F. Y. Yuan, C. S. Lin, Y. Z. Huang, H. Zhang, A. Y. Zhou, G. L. Chai and W. D. Cheng, $BaCdGeSe_4$: Synthesis, structure and nonlinear optical properties, *J. Solid State Chem.*, 2021, **302**, 122352; (*q*) H. S. Wang, X. T. Pan, W. Zhao, Y. Chu and J. J. Li, A new infrared nonlinear optical material $BaZnGeS_4$ with a wide band gap and large nonlinear optical response, *Inorg. Chem. Front.*, 2023, **10**, 6253; (*r*) C. L. Teske, Preparation and crystal-structure of barium-mercury-thiostannate (IV), $BaHgSnS_4$, *Z. Naturforsch., B: J. Chem. Sci.*, 1980, **35**, 7; (*s*) W. L. Yin, A. K. Iyer, C. Li, J. Y. Yao and A. Mar, Noncentrosymmetric chalcogenides $BaZnSiSe_4$ and $BaZnGeSe_4$ featuring one-dimensional structures, *J. Alloys Compd.*, 2017, **708**, 414.

25 S. K. Kurtz and T. T. Perry, A powder technique for evaluation of nonlinear optical materials, *J. Appl. Phys.*, 1968, **39**, 3798.

26 M.-Y. Ran, S.-H. Zhou, W.-B. Wei, B.-X. Li, X.-T. Wu, H. Lin and Q.-L. Zhu, Rational Design of a Rare-Earth Oxychalcogenide $Nd_3[Ga_3O_3S_3][Ge_2O_7]$ with Superior Infrared Nonlinear Optical Performance, *Small*, 2023, **19**, 2300248.

27 J. J. Xu, K. Wu, Y. Xiao, B. B. Zhang, H. H. Yu and J. H. Zhang, Mixed-Anion-Oriented Design of $LnMGa_3S_6O$ (Ln = La, Pr, and Nd; M = Ca and Sr) Nonlinear Optical Oxysulfides with Targeted Property Balance, *ACS Appl. Mater. Interfaces*, 2022, **14**, 37967.

28 D. J. Mei, W. Z. Cao, N. Z. Wang, X. X. Jiang, J. Zhao, W. K. Wang, J. H. Dang, S. Y. Zhang, Y. D. Wu and P. H. Rao, Breaking through the "3.0 eV wall" of energy band gap in mid-infrared nonlinear optical rare earth chalcogenides by charge-transfer engineering, *Mater. Horiz.*, 2021, **8**, 2330.

29 X. Tian, Y. Xiao, B. Zhang, D. Yang and K. Wu, Novel structural transformation in $K_3ReP_2S_8$ thiophosphates originating from the rare-earth (Re) cation sizes induced local coordination asymmetry, *Mater. Today Phys.*, 2022, **28**, 100885.

30 Y. X. Han, C. L. Hu and J. G. Mao, $Ca_2Ln(BS_3)(SiS_4)$ (Ln = La, Ce, and Gd): Mixed Metal Thioborate-Thiosilicates as Well-Performed Infrared Nonlinear Optical Materials, *Small*, 2024, **20**, 2305828.

31 M. J. Zhang, X. M. Jiang, L. J. Zhou and G. C. Guo, Two phases of Ga_2S_3: promising infrared second-order nonlinear optical materials with very high laser induced damage thresholds, *J. Mater. Chem. C*, 2013, **1**, 4754.

32 M.-Y. Ran, S.-H. Zhou, B.-X. Li, X.-T. Wu, H. Lin and Q.-L. Zhu, Balanced IR Nonlinear Optical Performance Achieved by Cation-Anion Module Cosubstitution in V-Based Salt-Inclusion Oxychalcogenides, *Chem. Mater.*, 2024, **36**, 11996.

33 Y. Huang, D. Chu, Y. Zhang, C. Xie, G. Li and S. Pan, Structure Prediction-Oriented Synthesis of Thiophosphates

as Promising Infrared Nonlinear Optical Materials, *Angew. Chem., Int. Ed.*, 2024, **63**, e202406576.

34 Y.-X. Han, C.-L. Hu, Z. Fang, Q.-Q. Chen, B.-X. Li, Y. Lin and J.-G. Mao, $LaBS_3$ revisited: a promising mid-infrared nonlinear optical material, *J. Mater. Chem. C*, 2022, **10**, 12556–12559.

35 R. Wang, F. Liang, X. Liu, Y. Xiao, Q. Liu, X. Zhang, L. M. Wu, L. Chen and F. Huang, Heteroanionic Melilite Oxysulfide: A Promising Infrared Nonlinear Optical Candidate with a Strong Second-Harmonic Generation Response, Sufficient Birefringence, and Wide Bandgap, *ACS Appl. Mater. Interfaces*, 2022, **14**, 23645–23652.

36 (*a*) G. Kresse, *VASP, 5.3.5*; **https://cms.mpi.univie.ac.at/vasp/vasp/vasp.html**; (*b*) G. Kresse and J. Furthmuller, Efficient iterative schemes for ab initio total-energy calculations using a plane-wave basis set, *Phys. Rev. B: Condens. Matter*, 1996, **54**, 11169; (*c*) G. Kresse and D. Joubert, From ultrasoft pseudopotentials to the projector augmented-wave method, *Phys. Rev. B: Condens. Matter*, 1999, **59**, 1758.

37 D. A. Kleinman, Nonlinear Dielectric Polarization in Optical Media, *Phys. Rev.*, 1962, **126**, 1977.

38 (*a*) Y.-F. Shi, Z. Ma, B.-X. Li, X.-T. Wu, H. Lin and Q.-L. Zhu, Phase matching achieved by isomorphous substitution in IR nonlinear optical material $Ba_2SnSSi_2O_7$ with an undiscovered $[SnO_4S]$ functional motif, *Mater. Chem. Front.*, 2022, **6**, 3054–3061; (*b*) M.-Y. Li, Z. Ma, B.-X. Li, X.-T. Wu, H. Lin and Q.-L. Zhu, $HgCuPS_4$: An Exceptional Infrared Nonlinear Optical Material with Defect Diamond-like Structure, *Chem. Mater.*, 2020, **32**, 4331–4339.

39 (*a*) H. Lin, Y.-Y. Li, M.-Y. Li, Z. Ma, L.-M. Wu, X.-T. Wu and Q.-L. Zhu, Centric-to-acentric structure transformation induced by a stereochemically active lone pair: a new insight for design of IR nonlinear optical materials, *J. Mater. Chem. C*, 2019, **7**, 4638; (*b*) Y. Xiao, M.-M. Chen, Y.-Y. Shen, P.-F. Liu, H. Lin and Y. Liu, $A_3Mn_2Sb_3S_8$ (A = K and Rb): A new type of multifunctional infrared nonlinear optical material based on unique three-dimensional open frameworks, *Inorg. Chem. Front.*, 2021, **8**, 2835–2843.

40 (*a*) C. Aversa and J. E. Sipe, Nonlinear optical susceptibilities of semiconductors: Results with a length-gauge analysis, *Phys. Rev. B: Condens. Matter Mater. Phys.*, 1995, **52**, 14636; (*b*) S. N. Rashkeev, W. Lambrecht and B. Segall, Efficient ab initio method for the calculation of frequency-dependent second-order optical response in semiconductors, *Phys. Rev. B: Condens. Matter Mater. Phys.*, 1998, **57**, 3905.

